06

Investigation of the filament properties in the HfO_2-based structures using conductive atomic force microscopy

© A.G. Isaev,[1,2] O.O. Permiakova,[1,2] A.E. Rogozhin[1]

[1] Valiev Institute of Physics and Technology, Russian Academy of Sciences, Moscow, Russia
[2] Moscow Institute of Physics and Technology (State University), Dolgoprudnyi, Moscow oblast, Russia
e-mail: isaev.ag@phystech.edu

Received January 18, 2023
Revised May 19, 2023
Accepted June 16, 2023

The results of the research on the resistive switching in $Pt/HfO_2/HfO_xN_y/TiN$, $Pt/HfO_2/TaO_xN_y/TiN$ and $Pt/Al_2O_3/HfO_2/TaO_xN_y/TiN$ structures are presented. Active layers of the structures were deposited by atomic layer deposition. The formation of conductive filaments in all three structures was demonstrated using conductive atomic force microscopy. A full cycle of resistive switching with a microscope probe in these structures was also demonstrated. The properties of filaments formed at different voltages were studied, and the distributions of the filament density by conductivity and size were presented. The characteristics of the studied structures were compared. It appears that the $Pt/Al_2O_3/HfO_2/TaO_xN_y/TiN$ structure has the greatest potential for resistive random-access memory application.

Keywords: memristor, resistive switching, resistive random-access memory, conductive atomic force microscopy.

DOI: 10.61011/TP.2023.08.57266.9-23

Introduction

In the near future, nanoelectronics will face difficulties in scaling traditional types of memory. It is necessary to develop new types of memory that make it possible to achieve greater element density with same high other characteristics, such as read and write speeds, power consumption and information storage time. One of the most promising candidates for the role of such memory seems to be resistive random access memory (ReRAM) [1]. Such memory can be implemented on the basis of memristor metal–insulator–metal (MIM) structures in which resistive switching (RS) is possible — cyclic change in electrical resistance between stable states under the influence of an electric field. The change in cell resistance occurs due to the formation of conductive filaments in the insulator layer. A state with high resistance corresponds to a logical zero, and the state with low resistance corresponds to one. ReRAM can potentially provide high density of structures (single cell size can be less than 10 nm) [2,3], write time — less than 1 ns [4], endurance — more than 10^9 [5], information storage time — more than 10 years, and power consumption less than 1 pJ per cell [2]. Despite the fact that a number of ReRAM prototypes was already presented, there are a number of problems that prevent the mass use of ReRAM, including the lack of structures that would simultaneously satisfy all requirements for characteristics, and a significant characteristics variations from cell to cell and over time [8]. Today, the most promising materials are hafnium and tantalum oxides. In structures based on these materials both subnanosecond switching [4,9], and a endurance exceeding 10^9 [5,10,11] were achieved. It was shown that bilayer structures based on hafnium and tantalum oxides can exhibit better switching characteristics than structures based on only one of these materials [12]. To reduce the characteristics variations, some studies used an additional ultrathin layer of aluminum oxide located at the interface with one of the electrodes [13,14]. This layer allows for better localization of filaments, thereby reducing the characteristics variations, and also increases the resistance ratio. The formation of oxide layers by atomic layer deposition (ALD) ensures high homogeneity of structures, thereby also reducing variations in characteristics [15,16]. Thus, multilayer structures based on hafnium, tantalum and aluminum oxides formed by the ALD method appear to be promising candidates for ReRAM application. To better evaluate the prospects of such structures, it is necessary to determine the mechanisms of RS in them and to study the properties of the conducting filaments due to which RS occurs. In this paper, for these purposes conductive atomic force microscopy (CAFM) was used, i.e. a widely used method for studying such structures [17].

1. Methods for the formation and study of memristor structures based on hafnium and tantalum oxides

To study the mechanisms of resistive switching in structures based on hafnium and tantalum oxides, three types of structures were fabricated: $HfO_2/HfO_xN_y/TiN$, $HfO_2/TaO_xN_y/TiN$ and $Al_2O_3/HfO_2/TaO_xN_y/TiN$ (hereinafter structures M1, M2 and M3, respectively). A bottom electrode of titanium nitride 200 nm thick was deposited onto a silicon wafer 650 μm thick using DC reactive magnetron sputtering. Then, another 5 nm of titanium

Table 1. Composition of the active layer for structures M1, M2, M3

M1	–	2 nm HfO_2	4 nm HfO_xN_y
M2	–	2 nm HfO_2	4 nm TaO_xN_y
M3	0.5 nm Al_2O_3	1.5 nm HfO_2	4 nm TaO_xN_y

nitride, as well as an active layer with a total thickness of 6 nm, were formed using ALD method (Table 1). For the deposition of HfO_2 thermal ALD was used at a temperature of 300°C, precursors — TEMAH and water vapor. The deposition of hafnium and tantalum oxides with an increased concentration of oxygen vacancies was carried out using plasma-stimulated ALD at a temperature of 300°C, precursors — TEMAH (hafnium oxide)/TBTDET (tantalum oxide) and hydrogen plasma. For the deposition of Al_2O_3 thermal ALD was used at temperature of 300°C, precursors — TMA and water vapor. To measure the I-V characteristics the top platinum electrodes (diameter 200 μm and thickness 100 nm) were deposited by magnetron sputtering through a shadow mask.

When studying I-V characteristics of structures with a top electrode, Keithley 4200-SCS system was used. To study the mechanisms of RS, the CAFM method was used, implemented in microscope, model SMM-2000. A microscope probe with a conductive platinum coating Golden Silicon Probes CSG01/Pt was used as the top electrode of the structures, force constant 0.003–0.13 N/m, tip radius 35 nm. Scanning time was 12 min, image size $2.1 \times 2.1\,\mu m^2$ (512×512 pixels). The scanning was carried out in the atmosphere. CAFM images were processed in SMM-2000 analysis program. Since currents up to 25 pA (current noise) were observed with CAFM probe withdrawn, regions, in which the measured current was less than 30 pA, were considered non-conducting; areas, where the current ranged from 30 pA to 12 nA, were considered conductive. When studying the distribution of the number of filaments based on the measured current value, the maximum obtained current value for each specific filament was taken into account. When studying filament sizes, median filtering was used to reduce the influence of noise on the size and shape of the filament cross-section.

2. Study of I-V characteristics of structures based on hafnium and tantalum oxides

For all structures M1-M3 the I-V characteristics of bipolar resistive switching were obtained, Fig. 1. The main RS characteristics are given in the Table 2. In all three structures, low operating voltages of less than 1V were obtained. The forming voltages in structures M2 and M3 were about 3V; in M1 it was significantly higher. The best

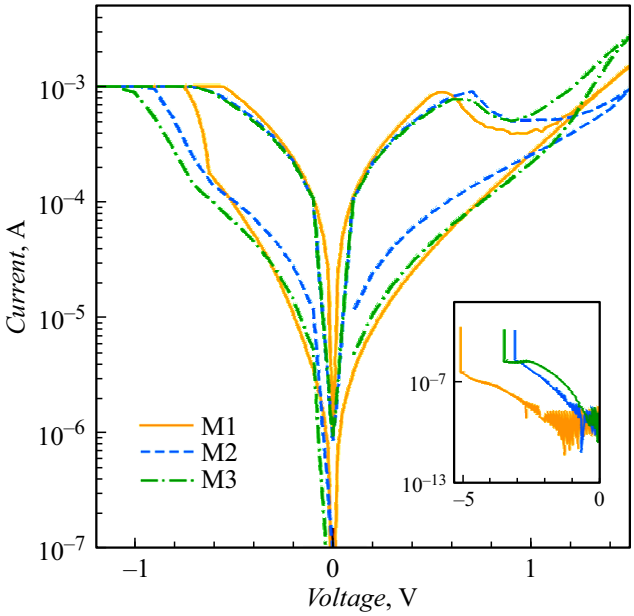

Figure 1. I-V characteristics of RS and electroforming of structures $Pt/HfO_2/HfO_xN_y/TiN$, $Pt/HfO_2/TaO_xN_y/TiN$, and $Pt/Al_2O_3/HfO_2/TaO_xN_y/TiN$.

Table 2. I-V characteristics of RS for structures M1, M2, M3

Structure	M1	M2	M3
Average forming voltage, V	−5	−3.3	−3.1
Set voltage, V	−0.7	−0.74	−0.87
Reset voltage, V	0.52	0.68	0.65
Resistance ratio	18	9	20

resistance ratio was obtained in M3 structure due to the ultra-thin layer of aluminum oxide.

3. Study of resistive switching mechanisms using CAFM

Fig. 2 shows an AFM image of the surface topography of three structures. For all studied structures, the root-mean-square surface roughness was less than 1 nm. Low surface roughness of the oxide layer was achieved through the use of the ALD method.

Resistive switching was performed by scanning the sample area with CAFM probe at a given voltage. The forming voltage was selected by successive scans with voltage increasing on the probe by absolute value in steps of 0.25 V. Electroforming of sample M1 occurred at voltages from −5 V. Moreover, during successive scans in the same region with voltage increasing, the number of filaments was significantly lower than absolute value simultaneous changes in the scanning region and voltage (Fig. 3, *a, b*). This effect was also observed in two other samples. The reason for this effect may be the death of oxygen vacancies during

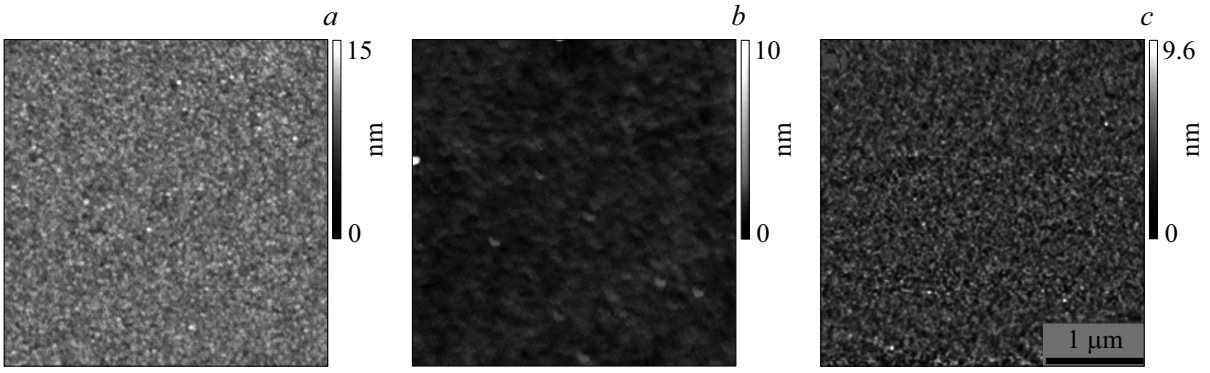

Figure 2. AFM Image of structure surface: *a* — $HfO_2/HfO_xN_y/TiN$, *b* — $HfO_2/TaO_xN_y/TiN$, *c* — $Al_2O_3/HfO_2/TaO_xN_y/TiN$.

interaction with the atmosphere or local anodic oxidation of the sample surface in a humid atmosphere with a negative voltage on the probe. These versions are confirmed by the fact that in structures where the active region is covered by the top electrode, this effect was not observed.

To make sure that the observed filaments were formed due to reversible resistive switching, state readings were taken, and one switching cycle was demonstrated. First, electroforming was performed at -5 V (Fig. 3, *c*). The resulting state was then read at -4 V to confirm the reproducibility of the filaments. Reading at lower voltages failed, probably due to oxidation of the upper part of the filament in the atmosphere. Some of the filaments formed at -5 V were reproduced at voltage -4 V (Fig. 3, *d*). Then a part of the area was „reset" by scanning at three different positive voltages with a sequential area increasing, as shown in Fig. 3,*e*. At that, when scanning with positive voltages, no conducting regions were observed. Moreover, the state reading showed that in the region subjected to „reset", all filaments disappeared (Fig. 3, *e*). After second set at -5 V it is clear that in the region scanned at $+2$ V, the filaments were restored, while the regions scanned at $+4$ and 5 V remained completely non-conductive (Fig. 3,*f*). Thus, too high reset voltages can lead to complete rupture of the filament. Higher forming voltages are presumably required for filament recovery.

Electroforming in the structure M2 was observed at voltages from -4.5 V. At positive voltage, no conductive filaments were observed in both regions subjected to electroforming, and regions not subjected to electroforming, this indicates the reset process. Thus, the appearance of conducting filaments is due to bipolar resistive switching.

Electroforming in M3 structure occurred at voltages from 4V̇. The reproducibility of the formed filaments was confirmed. Many filaments formed at -4.75 V were reproduced when reading from -4.5 V, as shown in Fig. 3, *g, h*. Also, „reset" was performed at different voltages (2. 3.5 and 5 V) followed by „second set" at -4.75 V (Fig. 3, *i*). At all positive voltages considered there was no conductivity, this indicates a successful „reset,,. During „second set" in the region „reset" at $+5$ V, the filaments were not fully restored. In the regions where „reset" was carried out at $+2$ and $+3.5$ V part of the filaments was restored, which indicates successful „second set".

In all three structures, the appearance of conducting regions was observed when scanning with negative voltages, and they disappeared when scanning with positive voltages. Based on these results, as well as many studies in which filamentary RS was observed in structures based on hafnium and tantalum oxides [18–23], we can conclude that there is a filamentary switching mechanism in structures M1–M3. Nonfilamentary mechanisms were observed mainly in semiconductor oxides with a perovskite structure [24], to which hafnium and tantalum oxides do not belong. The main mechanisms of filament formation in memristors based on transition metal oxides are oxygen vacancy migration (VCM), active electrode ion migration (ECM), or thermochemical mechanism (TCM) [1]. The latter mechanism, usually, is found in memristors based on semiconductor oxides (for example, titanium oxide [25]), and is accompanied by unipolar RS. As bipolar RS was observed in the M1–M3 structures, this mechanism can be excluded. The ECM mechanism was observed in structures based on hafnium and tantalum oxides [21,23], however, both titanium nitride and platinum are poorly suited for the role of active electrode, so this mechanism is also unlikely. Thus, the most likely mechanism is the migration of oxygen vacancies, which is widely found in such structures [18–20]. Nevertheless, the effects at the interfaces between various oxides were poorly studied and require further study.

To study the dependence of the spatial distribution density of filaments on the forming voltage, the electroforming of samples M1–M3 was performed at different voltages (Fig. 4). In structure M1 (Fig. 4, *a–c*) at forming voltages -5 , -5.25 and -5.5 V the filament density also increases as the voltage increases. At voltage -5.75 V the influence of probe degradation is noticeable, especially in the lower part of the image, so only the upper half of the image was taken into account when calculating statistics. In structure M2 electroforming was observed at lower voltages than in M1, so the density and conductivity of the filaments turned out to be noticeably lower (Fig. 4, *d–f*). Another

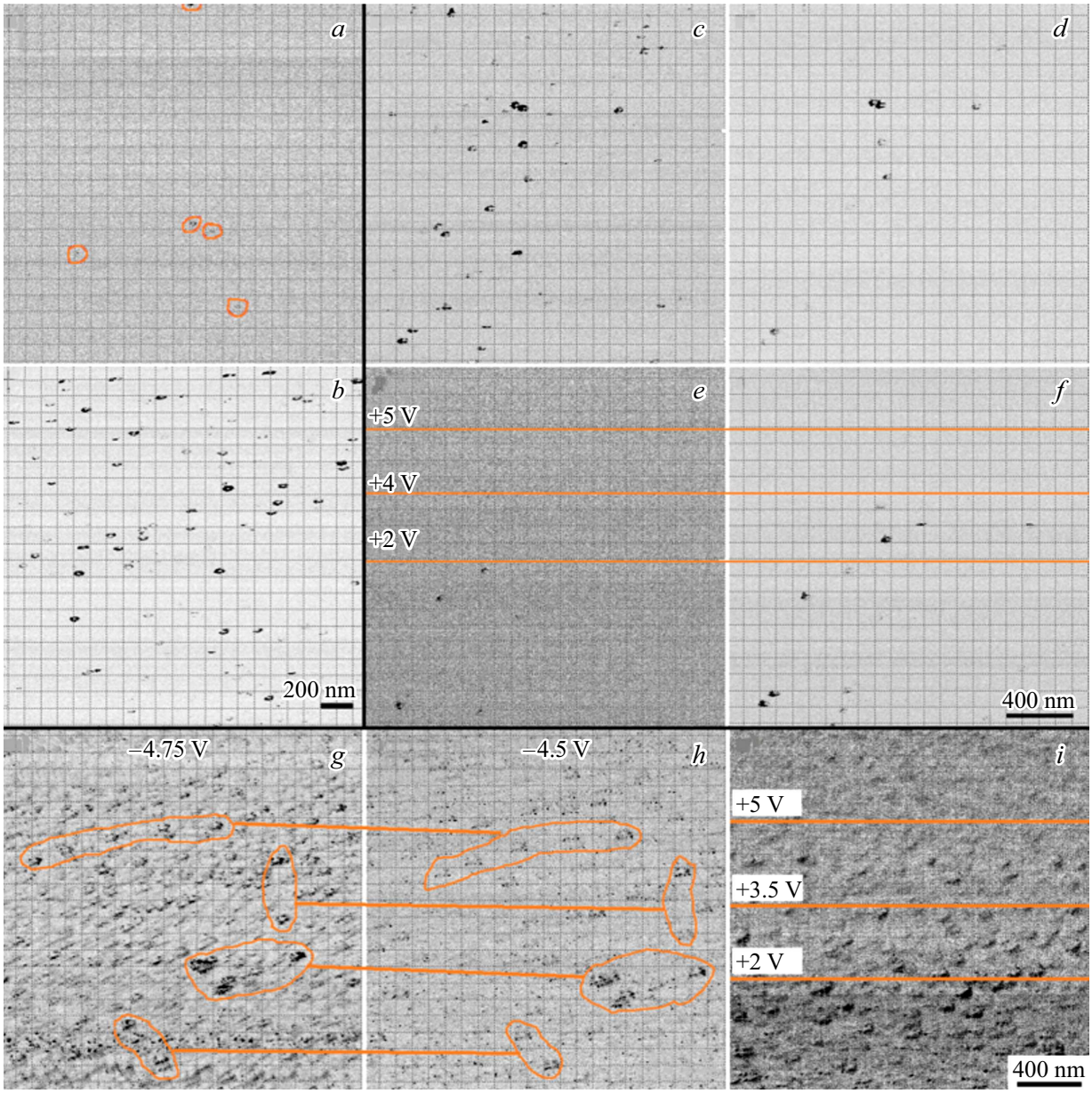

Figure 3. CAFM images showing filament formation in various structures. Gray areas are considered non-conductive, black areas are considered conductive filaments. CAFM images obtained during electroforming at −5 V region of the structure subjected to successive scans by increasing voltage from −4.5to −5 V (*a*) and a new area that was not scanned at lower voltages (*b*); CAFM images of complete switching cycle in structure $HfO_2/HfO_xN_y/TiN$: electroforming at −5 V (*c*), reading at −4 V (*d*), reset the state at −4 V after „reset" of the part of the area at different voltages (+2, +4, +5 V) (*e*) set at −5 V (*f*); CAFM images of one region of the sample $Al_2O_3/HfO_2/TaO_xN_y/TiN$ at different voltages: filaments formed at −4.75 V (*g*) are reproduced at lower voltage (*h*), CAFM image of the sample $Al_2O_3/HfO_2/TaO_xN_y/TiN$ obtained with −4.75 V, after a series of scans at different „reset" voltages (*i*).

important feature of M2 structure is the presence of large filaments formed on large protruding grains. In structure M3 electroforming was observed at the lowest voltages of all three structures. At voltage −4.75 V a significant increase in the number of filaments was observed compared to −4.5 V (Fig. 4, *g*–*i*).

Based on the data obtained, distributions of the number of filaments in the field $2 \times 2\,\mu$m were plotted depending on their conductivity, expressed in the maximum current value through the filament for four electroforming voltages (Fig. 5, *a, c, e*), and the distribution of the area fraction with given current value at different voltages (Fig. 5, *b, d, f*). In M1 structure, in most cases, the increase in voltage leads to increase in the number of filaments in each conductivity range. Also the area of conducting regions increases. In all four considered ranges, a similar number of filaments was obtained, but the total area of regions with high conductivity is significantly less than the total area

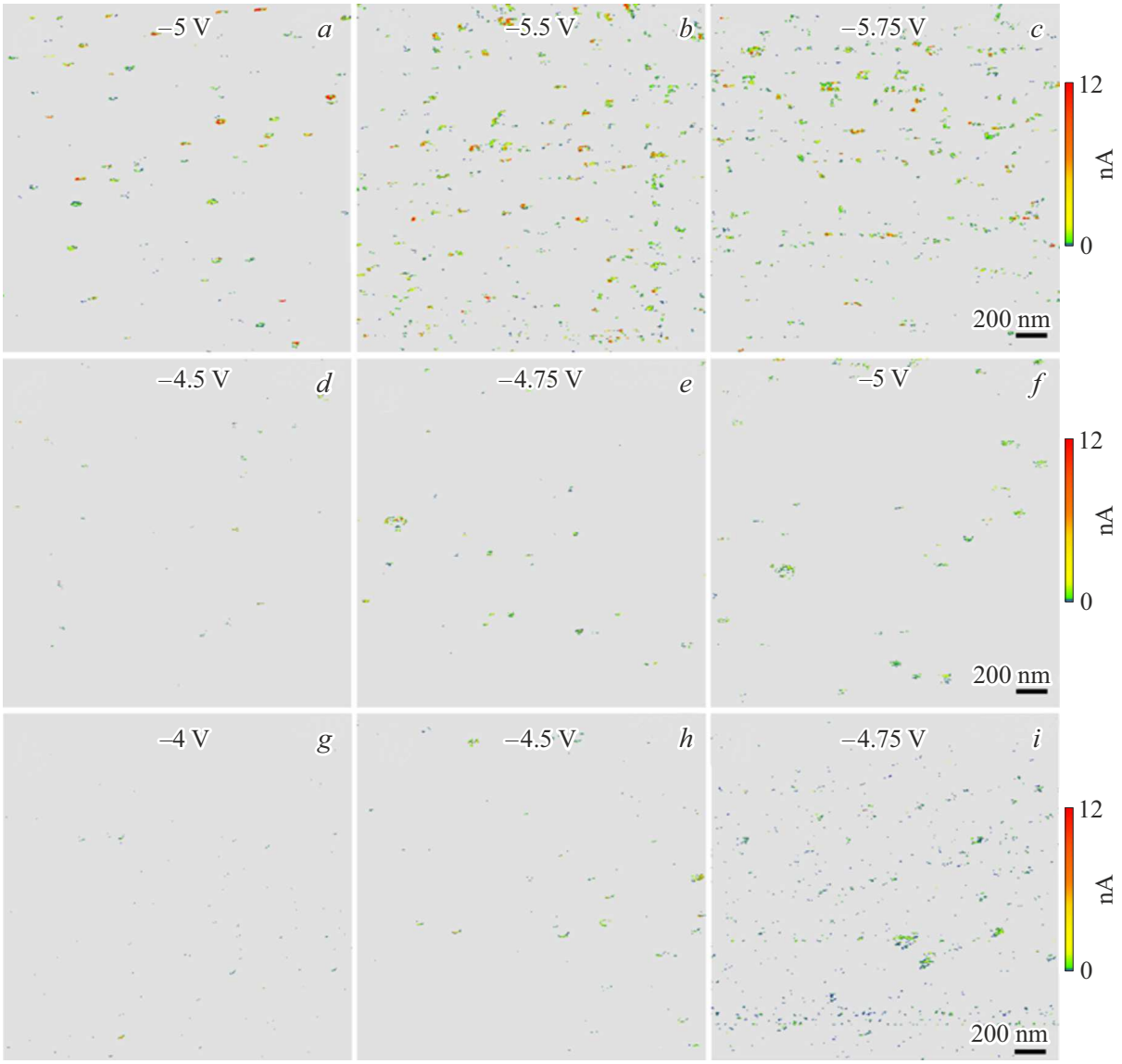

Figure 4. CAFM images obtained during structure electroforming: *a–c* — $HfO_2/HfO_xN_y/TiN$ at voltages from −5 to −5.75 V; *d–f* — $HfO_2/TaO_xN_y/TiN$ at voltages from −4.5 to −5 V, *g–i* — $Al_2O_3/HfO_2/TaO_xN_y$ /TiN at voltages from −4 to −5.75 V. Non-conducting areas with measured current less than 30 pA are indicated in gray; colors from blue to red (in the online version) indicate areas of filaments with different measured currents.

of regions with medium and low conductivity (Fig. 5, *b*). This effect is explained by the fact that in the CAFM image, parts of the filaments near the boundary have lower conductivity than the central part, probably due to the features of measurements using CAFM. For structure M2 the distributions are slightly shifted towards low currents. With voltage increasing there is a slight increase in the number of filaments. For the distribution over area there is a noticeable increase in area for both higher voltages and lower conductivities. Thus, with voltage increasing there is a the size of the filaments predominantly increase, but not their number. In structure M3 filaments with weak conductivity prevail. This may be due to lower forming stresses compared to other samples. As the voltage increases, there is a commensurate increase in the number of filaments and their total area.

Figure 6 shows the filament cumulative distribution function by the area. For M1, about 50% of filaments have area less than 300 nm ^{2}. At voltage −5 V the areas of about 25% of the filaments lie in the range 700−1400 nm^2. At higher voltages the distributions have a similar shape, with about 80% of the filaments having area less than 600 nm^2. In M2 with voltage increasing the increase in the size of the filaments was observed. The median value of the filament area was 230, 470 and 590 nm^2, in 90% of filaments the area did not exceed 1130, 1350 and 1950 nm^2 for voltages −4.5, −4.75 and −5 V respectively. These results also indicate that for the M2 sample the filament

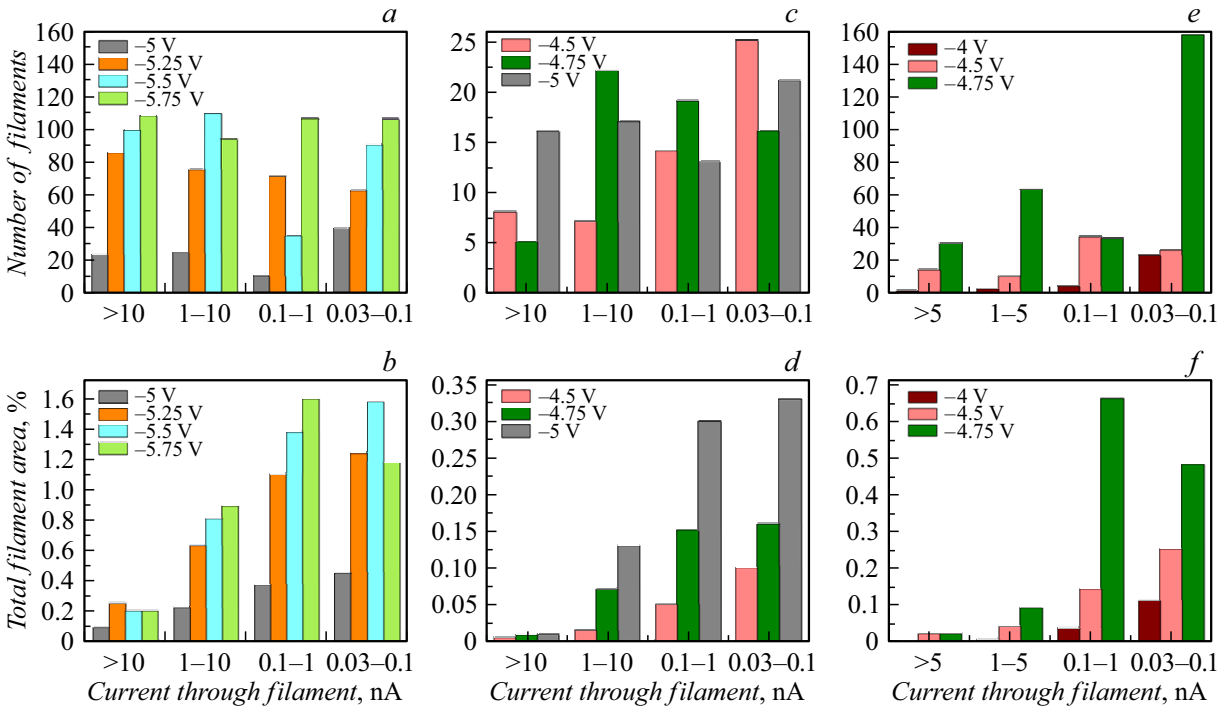

Figure 5. Distributions at different electroforming voltages: *a* — number of filaments by conductivity and *b* — total fraction of the area of given conductivity in the structure $HfO_2/HfO_xN_y/TiN$; *c* — number of filaments by conductivity and *d* — total fraction of the area of given conductivity in the structure $HfO_2/TaO_xN_y/TiN$; *e* — number of filaments by conductivity and *f* — total fraction of the area of given conductivity in the structure $Al_2O_3/HfO_2/TaO_xN_y/TiN$. Filament conductivity is expressed in terms of the measured current through the filament.

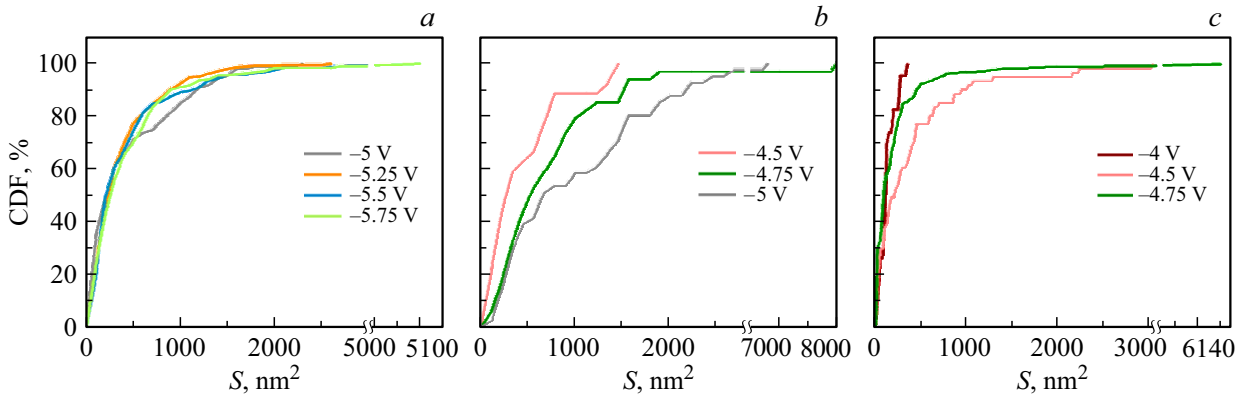

Figure 6. The filament cumulative distribution function by the area for structures: *a* — $HfO_2/HfO_xN_y/TiN$, *b* — $HfO_2/TaO_xN_y/TiN$, *c* — $Al_2O_3/HfO_2/TaO_xN_y/TiN$.

sizes increase with voltage increasing. In M3 at −4 V the largest filaments have area of 350 nm^2. At −4.5 V more than 50% of filaments have area less than 200 nm^2, but about 40% of filaments lie in the range from 300 to 1100 nm^2. At −4.75 V the distribution is steeper, median value — 90 nm^2, 90% of filaments do not exceed 450 nm^2.

Table 3 shows summary data for all three structures. M2 structure has the least roughness, but the presence of individual large protruding grains can lead to significant variations in switching characteristics from cell to cell when applying in ReRAM. Structures M1 and M3 also have an acceptable roughness of less than 1 nm, while having better surface homogeneity. Structure M1 requires the highest forming voltages; in structure M3 electroforming is possible at the lowest voltages. The lower currents flowing through the filaments in M3 structure may provide potentially lower power consumption, however, they may be associated with lower voltages during electroforming. In structure M2 a lower concentration of filaments was observed than in the other two structures at equal voltages (−5 V for M1 and −4.75 V for M3). In structure M1 at −5.75 V the highest concentration of filaments is observed. However,

Table 3. Comparison of results obtained for structures M1, M2, M3

Structure		M1		M2		M3
Root-mean-square roughness, nm		0.93		0.49		0.83
Minimum forming voltage, V		−5		−4.5		−4
Relative conductivity of filaments		High		Mean		Low
Forming voltage, V		−5	−5.75	−4.75	−5	−4.75
Total number of filaments on scan		96	414	54	67	283
Average cell size per one filament, nm		225	108	299	269	131
Area fraction covered by filaments, %		1.13	3.87	0.17	0.77	1.25
Median value	of filament cross-sections, nm	22	20	29	44	14
	filaments areas, nm^2	205	250	465	590	90
The value within which 90%	of filament cross-section sections lie, nm	63	48	49	80	38
	of filament areas lie, nm^2	1170	900	1350	1950	450

in structure M3 at −4.75 V the concentration of filaments is higher than in M1 at −5 V, i.e. at equal voltages the structure M3 has the potential to provide the highest concentration of filaments. For high integration density in ReRAM, smaller sizes of filaments are preferred. M3 structure provides significantly smaller sizes of filament. It is also important to note that reducing the scanning area CAFM with resolution increasing and scanning speed decreasing can potentially lead to a further reduction in the size of the resulting filaments, as well as increase in their density.

Thus, M3 structure is superior to other structures in almost all main characteristics. It provides optimal surface topography, lowest forming voltage, higher density and smaller filament size. Consequently, three-layer structures based on 0.5 nm aluminum oxide, 1.5 nm hafnium oxide and 4 nm tantalum oxide from the considered structures have the greatest potential for use in ReRAM.

Conclusion

The work studied the mechanisms of resistive switching in memristor structures based on hafnium and tantalum oxides to evaluate the prospects for these structures use in the creation of ReRAM. Three types of memristor structures were formed: $HfO_2/HfO_xN_y/TiN$, $HfO_2/TaO_xN_y/TiN$ and $Al_2O_3/HfO_2/TaO_xN_y/TiN$. Oxide layers with a total thickness of 6 nm were formed by ALD. The resulting samples were studied using AFM with conducting probe. The root mean square surface roughness for all types of structures was less than 1 nm. For all types of structures, it was possible to achieve the formation of conducting filaments using the CAFM probe. The reproducibility of the filaments at different voltages and the full cycle of bipolar switching with the CAFM probe were demonstrated. The filamentous switching mechanism based on the migration of oxygen vacancies in the oxide was confirmed. In structures $HfO_2/HfO_xN_y/TiN$, $HfO_2/TaO_xN_y/TiN$ and $Al_2O_3/HfO_2/TaO_xN_y/TiN$ forming was observed at probe voltages of −5, −4.5 and −4 V, respectively. With voltage increasing, an increase in filament density was observed. The cell size, per which on average one filament occurs, was 108, 269 and 131 nm at voltages −5.75, −5 and −4.75 V in structures $HfO_2/HfO_xN_y/TiN$, $HfO_2/TaO_xN_y/TiN$ and $Al_2O_3/HfO_2/TaO_xN_y/TiN$ respectively. At equal voltages in the structure $Al_2O_3/HfO_2/TaO_x$ N_y/TiN the highest filament density can be potentially obtained. Filaments of smaller size than in the other two structures were also observed in this structure. Based on the results obtained, the structure $Al_2O_3/HfO_2/TaO_xN_y/TiN$ has the greatest potential of the studied structures for use in the creation of ReRAM.

Funding

The study was performed under the state assignment to the Valiev Institute of Physics and Technology of RAS of the Ministry of Education and Science of the Russian Federation on the topic № FFNN-2022-0019.

Conflict of interest

The authors declare that they have no conflict of interest.

References

[1] F. Pan, S. Gao, C. Chen, C. Song, F. Zeng. Mater. Sci. Engineer.: R: Reports, **83**, 1 (2014). DOI: 10.1016/j.mser.2014.06.002

[2] B. Govoreanu, G. Kar, Y.Y. Chen. In Proc. IEDM IEEE Intern., Washington, DC, USA (2011), p. 31.6.1. DOI: 10.1109/IEDM.2011.6131652

[3] S. Pi, C. Li, H. Jiang, W, Xia, H. Xin, J. Yang. Nature Nanotechnology, **14**, 35 (2019). DOI: 10.1038/s41565-018-0302-0
[4] A.C. Torrezan, J.P. Strachan, G. Medeiros-Ribeiro. Nanotechnology, **22**, 485203 (2011). DOI: 10.1088/0957-4484/22/48/485203
[5] M.-J. Lee, C.B. Lee, D. Lee, S.R. Lee, M. Chang, J.H. Hur. Nature Mater., **10**, 625 (2011). DOI: 10.1038/nmat3070
[6] T. Liu, T.H. Yan, R. Scheuerlein. In Proc. IEEE J. Solid-State Circuits, **49**, 140 (2014). DOI: 10.1109/JSSC.2013.2280296
[7] R. Fackenthal, M. Kitagawa, W. Otsuka, K. Prall, D. Mills, K. Tsutsui. In Proc. IEEE ISSCC (San Francisco, USA, 2014). p. 338. DOI: 10.1109/ISSCC.2014.6757460
[8] M. Lanza, H.-S.P. Wong, E. Pop, D. Ielmini, D.I. Strukov, B.C. Regan. Adv. Electron. Mater., **5**, 1800143 (2019). DOI: 10.1002/aelm.201800143
[9] H.Y. Lee, Y.S. Chen, P.S. Chen. In Proc. IEEE IEDM (San Francisco, USA, 2010), p. 19.7.1. DOI: 10.1109/IEDM.2010,5703395
[10] S. Koveshnikov, K. Matthews, K. Min, D. C. Gilmer, M.G. Sung, S. Deora. In Proc. IEEE IEDM (San Francisco, USA, 2012), p. 20.4.1. DOI: 10.1109/IEDM.2012.6479080
[11] A.V. Fadeev, K.V. Rudenko. Russ. Microelectron., **50**, 311 (2021). DOI: 10.1134/S1063739721050024
[12] M.R. Park, Y. Abbas, H. Abbas. Q. Hu, T.S. Lee, Y.J. Choi. Microelectron. Engineer., **159**, 190 (2016). DOI: 10.1016/j.mee.2016.03.043
[13] S. Biswas, A. Paul, P. Das P. Tiwary, H.J. Edwards, V.R. Dhanak. In Proc. IEEE Trans. Electron Devices, **68**, 3787(2021). DOI: 10.1109/TED.2021.3084554
[14] K.-M. Persson, S. Mamidala, L.-E. Wernersson. In Proc. IEEE J. Electron Devices Soc., **9**, 564 (2021). DOI: 10.1109/JEDS.2021.3079398
[15] Y.M. Chesnokov, A.V. Miakonkikh, A.E. Rogozhin, K.V. Rudenko, A.L. Vasiliev. J. Mater. Sci., **53**, 7214 (2018). DOI: 10.1007/s10853-018-2099-5
[16] C. Liu, C. Zhang, Y. Cao. J. Mater. Chem. C, **8**, 12478 (2020). DOI: 10.1039/D0TC02494E
[17] U. Celano (editor). *Electrical Atomic Force Microscopy for Nanoelectronics* (Springer International Publishing, 2019), DOI: 10.1007/978-3-030-15612-1
[18] S. Dirkmann, J. Kaiser, C. Wenger, T. Mussenbrock, ACS Appl. Mater. Interfac., **10** (17), 14857 (2018). DOI: 10.1021/acsami.7b19836
[19] S. Sharath, S. Vogel, L. Molina-Luna, E. Hildebrandt, C. Wenger, J. Kurian. Adv. Functional Mater., **27** (32), 1700432 (2017). DOI: 10.1002/adfm.201700432
[20] M.J. Lee, C. Lee, D. Lee, S. Lee, M. Chang, J. Hur. Nature Mater., **10** (8), 625 (2011). DOI: 10.1038/nmat3070
[21] H. Jiang, L. Han, P. Lin, Z. Wang, M.H. Jang, Q. Wu. Scientific Reports, **6** (1), 28525 (2016). DOI: 10.1038/srep28525
[22] F. Kurnia, C. Liu, C.U. Jung, B.W. Lee. Appl. Phys. Lett., **102** (15), 152902 (2013). DOI: 10.1063/1.4802263
[23] J.H. Yoon, J. Zhang, P. Lin, N. Upadhyay, P. Yan. Adv. Mater., **32** (9), 1904599 (2020). DOI: 10.1002/adma.201904599
[24] A. Sawa. Mater. Today, **11** (6), 28 (2008). DOI: 10.1016/S1369-7021(08)70119-6
[25] D.-H. Kwon, K.M. Kim, J.H. Jang, J.M. Jeon, M.H. Lee, G.H. Kim. Nature Nanotechnology, **5** (2), 148 (2010). DOI: 10.1038/nnano.2009.456

Translated by I.Mazurov